RSC Advances

PAPER

Cite this: *RSC Adv.*, 2021, **11**, 32622

An excellent water-stable 3D Zn-MOF with 8-fold interpenetrated diamondoid topology showing "turn-on/turn-off" luminescent detection of Al^{3+} and SNT in aqueous media†

Xiuting Gao,[a] Xiaohe Wang,[a] Miaomiao Feng,[a] Ming Yang[b] and Qingfu Zhang *[a]

The effective detection of Al^{3+} and antibiotics pollutants is crucial for environmental protection and human health due to their high toxicity and nondegradability, but it is still currently challenging. In this work, a methyl-decorated acylamide-containing dicarboxylate ligand H_2L was elaborately designed and successfully synthesized, which was further employed to react with Zn(II) ions and dpe ligands to construct a new luminescent Zn-MOF, namely $\{[Zn(L)(dpe)]\cdot DMF\cdot 3H_2O\}_n$ (**1**). X-ray crystallography reveals that MOF **1** is a 3D 8-fold [4 + 4] interpenetrated diamondoid framework with isolated DMF and water molecules in the pores, in which the uncoordinated acylamide groups are found and facilitate the Zn-MOF to recognize analyte molecules. The activated solvent-free MOF sample (denoted as **1a**) exhibits excellent water stability and good luminescent performance. The luminescence sensing experiments show that **1a** could behave as a bi-responsive chemical sensor for "turn-on" and "turn-off" luminescent detection of Al^{3+} and SNT in aqueous media, respectively. The sensing mechanisms have also been discussed. Furthermore, MOF **1a** was successfully applied to the effective determination of Al^{3+} and SNT in real water samples. This represents, to our knowledge, the first example of a MOF material for "turn-on" and "turn-off" luminescent detection of Al^{3+} and SNT in water, which will promote the practical application of water-stable luminescent MOF sensors in monitoring metal ions and antibiotics pollutants in the environmental water matrices.

Received 1st September 2021
Accepted 27th September 2021

DOI: 10.1039/d1ra06590d

rsc.li/rsc-advances

Introduction

Trivalent aluminum ions (Al^{3+}) and antibiotics pollutants are becoming a serious global problem for harming the ecological environment and human health due to their high toxicity and nondegradability.[1–4] Al^{3+} is one of the common cations that can cause drinking water pollution. The excess Al^{3+} entering the human body would lead to severe illnesses including Alzheimer's disease and Parkinson's disease.[5,6] Similarly, the abuse of antibiotics such as sulfanitran (SNT) has brought about high level of antibiotic residue, although the antibiotics have been widely used for the treatment of bacterial infections in human beings and animals. The large amount of antibiotics residues in various aquatic environment would not only generate the drug resistance for microbial strains among mankind but also increase the risk of human carcinogenic and mutagenic diseases by bioaccumulation effect.[7–9] Currently, the inductively coupled plasma mass spectrometry (ICP-MS),[10] atomic absorption spectrometry (AAS)[11] and liquid chromatography tandem mass spectrometry (LC-MS)[12] are the conventional methods to detect Al^{3+} or antibiotics, but they exhibit some disadvantages such as complicated operation, expensive equipment, and time-consuming procedure. Therefore, it is urgent for scientists to develop a simple, inexpensive and time-saving approach for detection of Al^{3+} and SNT in water.

Luminescent metal–organic frameworks (MOFs), as a new type of crystalline materials, are obviously superior to other luminescent materials due to their excellent optical performance, permanent porosity, high surface area, and easily tailorable structures and functions.[13–15] Taking advantage of these unique merits, some luminescent MOFs have been successfully developed into "turn-on" and "turn-off" bi-responsive chemical sensors for detecting different pollutants including metal ions and/or organic pollutants *via* luminescence enhancing or luminescence quenching mechanism, respectively. For example, Wang and co-workers reported a luminescent 3D Cd-MOF behaving as a bi-responsive chemical sensor in DMF solutions for "turn-on" detecting Al^{3+} and Cr^{3+} as well as "turn-off" detecting Fe^{3+}, respectively.[16] Li group reported a highly

[a]College of Chemistry and Chemical Engineering, Liaocheng University, Liaocheng 252059, China. E-mail: zhangqingfu@lcu.edu.cn

[b]Fujian Institute of Research on the Structure of Matter, Chinese Academy of Sciences, Fuzhou 350002, China

† Electronic supplementary information (ESI) available: Crystallographic data, supplementary figures and tables. CCDC 2104369. For ESI and crystallographic data in CIF or other electronic format see DOI: 10.1039/d1ra06590d

luminescent 3D Zn-MOF acting as a bi-responsive chemical sensor for "turn-on" detecting toluene vapor and "turn-off" detecting nitrobenzene vapor, respectively.[17] Zhang *et al.* reported a luminescent 2D Zn-MOF serving as a bi-responsive chemical sensor in the aqueous phase for "turn-on" detecting Al^{3+} and "turn-off" detecting nitroaromatic explosives, respectively.[18] However, to our knowledge, no study on exploring MOF as "turn-on" and "turn-off" bi-responsive luminescent sensor for detecting Al^{3+} and antibiotics has been reported so far.

Water stability of luminescent MOFs in various water environment even acid and base aqueous solutions is key factor for practical applications.[19–21] Generally, there are two most common methods to improve the water stability of target MOFs. The first one is the use of high-valent metal ions to form strong coordination bonds with organic ligands.[22,23] The other one is the incorporation of hydrophobic groups around coordination sites of organic ligands to enhance the hydrophobic property of MOFs, and then to protect coordination bonds from hydrolysis.[24] In addition, a comparative study showed that the interpenetrated topological structure would also obviously enhance the water stability of target MOFs.[25,26]

In this work, a methyl-decorated acylamide-containing dicarboxylate ligand, 4,4′-((naphthalene-1,4-dicarbonyl) bis(azanediyl))bis(2-methylbenzoic acid) (H_2L), has been elaborately designed and successfully synthesized, in which two hydrophobic methyl groups are introduced into the *ortho*-position of the coordination carboxylate groups in order to enhance the water stability of target MOFs, as well as two acylamide groups are also introduced into H_2L ligands as guest-accessible functional organic sites (FOS) in order to improve their sensing ability. As expected, a new Zn-MOF $\{[Zn(L)(dpe)]\cdot DMF\cdot 3H_2O\}_n$ (**1**) was obtained by reaction of H_2L, $Zn(NO_3)_2\cdot 6H_2O$ and 1,2-di(pyridin-4-yl)ethane (dpe) under solvothermal condition. X-ray crystallography revealed that MOF **1** exhibited a 3D 8-fold [4 + 4] interpenetrated diamondoid framework with isolated DMF and water molecules in the pores. The activated solvent-free MOF sample **1a** was fabricated by the solvent-exchange and vacuum heat treatment technique, showing an enhanced stability in water, boiling water, as well as HCl and NaOH aqueous solution. The luminescence sensing experiments showed that **1a** could behave as a bi-responsive chemical sensor for "turn-on" and "turn-off" luminescent detection of Al^{3+} and SNT in aqueous media (Fig. 1). In addition, the "turn-on" and "turn-off" luminescent sensing mechanisms for Al^{3+} and SNT have also been discussed. To our knowledge, this represents the first example of bi-responsive MOF sensor for "turn-on" and "turn-off" luminescent detection of Al^{3+} and SNT in aqueous media.

Experimental section

Materials and measurements

All chemicals were of analytical grade and used without further purification. Elemental analyses for C, H, and N were carried out on an Elementar vario EL cube analyzer. Infrared spectra were recorded on a Nicolet-5700 FT-IR spectrophotometer with KBr pellets. Powder X-ray diffraction (PXRD) patterns were recorded on a Rigaku SmartLab 9 kW diffractometer with Cu Kα radiation (λ = 1.5418 Å) at room temperature. Thermogravimetric analyses (TGA) were performed under the nitrogen atmosphere on a Netzsch STA 449F5 thermal instrument. Adsorption isotherms for water vapor were measured with an Hiden intelligent gravimetric sorption analyzer at 298 K. The contact angle toward water was recorded with Krüss DSA 100S instrument. X-ray photoelectron spectroscopy (XPS) were performed on a Thermo Fisher Scientific Escalab Xi+ system. The absorption spectra were recorded on a Persée T9CS UV-Vis spectrophotometer. The photoluminescence spectra were measured on a Hitachi F-4700 spectrophotometer.

Synthesis of $\{[Zn(L)(dpe)]\cdot DMF\cdot 3H_2O\}_n$ (1)

A mixture of $Zn(NO_3)_2\cdot 6H_2O$ (29.8 mg, 0.1 mmol), H_2L (48.2 mg, 0.1 mmol) and dpe (18.4 mg, 0.1 mmol) in DMF/H_2O (3 mL, v/v = 1 : 2) was sealed in a Teflon-lined stainless steel vessel and heated at 120 °C for 3 days, and then cooled to room temperature at a rate of 5 °C h^{-1}. Colorless block crystals of MOF **1** were obtained with a 60.2% yield based on Zn(II). Elemental anal. calcd for $C_{43}H_{45}N_5O_{10}Zn$ (%): C, 60.25; H, 5.29; N, 8.17; anal. found: C, 60.23; H, 5.32; N, 8.21. Selected IR (KBr, cm^{-1}): 3423, 1664, 1615, 1525, 1383, 1311, 1253, 833, 793.

Sample activation of 1a

The as-synthesized sample of **1** was firstly immersed into anhydrous methanol for 3 days, and the methanol was refreshed three times each day. Then the similar procedure was utilized to treat the sample with dichloromethane to remove methanol molecules. After removal of dichloromethane by centrifuging, the sample was dried under vacuum at 80 °C for 12 h to yield activated solvent-free sample **1a**. Solid samples of **1a** were ground into powder and used for other measurements.

Luminescence measurements

In a typical luminescence experiment, 0.86 mg finely grounded powder of **1a** was added to a cuvette containing 10 mL deionized water, and then ultrasonicated for 8 h to form a uniform suspension. All the titration experiments were performed by adding the selected analytes to 1 mL of **1a** suspension. The luminescence spectra were recorded with an emission peak around 470 nm upon excitation at 340 nm. All the experiments were performed in triplicate, and the consistent results were reported.

DFT calculation

HOMO–LUMO energies were obtained using Materials Studio 7.0 version. In the DFT calculations, the exchange-correlation functional PW916 within the generalized gradient approximation (GGA) and the double numerical plus polarization (DNP) basis set as implemented in the DMol3 package of MS were used to optimize the geometries and evaluate the HOMO–LUMO energies of the analytes.

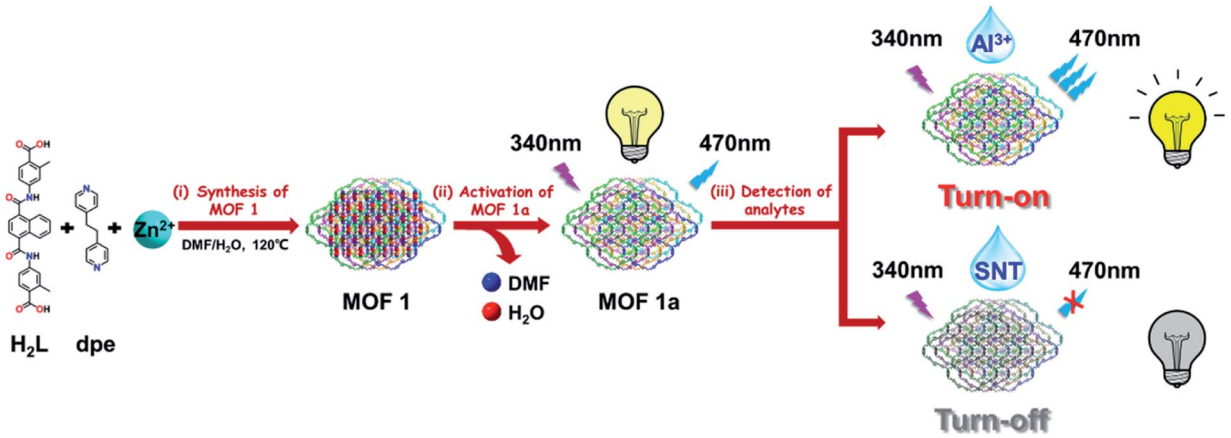

Fig. 1 Schematic diagram of luminescent MOF **1a** as a bi-responsive chemical sensor for "turn-on" and "turn-off" detection of Al^{3+} and SNT respectively, including (i) synthesis of pristine MOF **1**, (ii) activation of MOF **1a**, and (iii) detection of different analytes.

X-ray crystallography

Single-crystal X-ray diffraction data were collected on a Bruker SMART-1000 CCD diffractometer with graphite-monochromated Mo Kα (λ = 0.71073 Å) radiation at 298 K. The structure was solved by direct methods and refined by the full-matrix least-squares methods on F^2 using the SHELXL-2018 program.[27] Crystal and refinement data are summarized in Table S1.† Selected bond lengths and angles are listed in Table S2.†

Results and discussion

Description of crystal structure

Single-crystal X-ray diffraction analysis reveals that MOF **1** crystallizes in the monoclinic space group $P2_1/n$ and consists of one Zn(II) ion, one L^{2-} ligand, one dpe ligand, three isolated H_2O and one isolated DMF molecules in the asymmetric unit (Fig. S1†). In MOF **1**, the central Zn(II) ion (Zn1) is four-coordinated by two carboxylic O atoms (O1 and O6A, symmetry codes: A: $x-3/2, -y+1/2, z-1/2$) from two different L^{2-} ligands and two pyridyl N atoms (N3 and N4B, symmetry codes: B: $x-1/2, -y+3/2, z+1/2$) from two different dpe ligands, displaying a distorted $[ZnO_2N_2]$ tetrahedral coordination geometry. All the Zn–O and Zn–N lengths are in the normal range (Table S2†). The deprotonated L^{2-} ligand in **1** acts as a linear μ_2-bridging ligand with two monodentate coordination carboxylic O atoms, and the dpe also acts as a linear μ_2-bridging ligand with two coordination pyridyl N atoms (Fig. S2†). Interestingly, ten 4-connected tetrahedral Zn(II) centres are linked by six linear μ_2-bridging L^{2-} ligands and six linear μ_2-bridging dpe ligands to construct an diamondoid cage with a large internal pore diameter of 21.5 Å (Fig. 2a). These adjacent diamondoid cages *via* sharing 4-connected Zn(II) centres are further extended into form a 3D **dia** network, which possesses large pores (25.13 × 25.09 $Å^2$) along the crystallographic [10−1] direction (Fig. 2b). Due to the large pores in the single non-interpenetrated 3D network, eight such independent 3D networks interpenetrate with each other to form an 8-fold interpenetration structure in **1** (Fig. 2c). The detailed analyses show that the 8-fold interpenetrated structure in **1** can be best described as the [4 + 4] mode, in which a single network is interpenetrated by three other identical networks to form a 4-fold interpenetration network that then cross each other (Fig. 2d). As reported, the 8-fold interpenetration with [4 + 4] mode is rather rare.[28–31] In spite of the high level of interpenetration, MOF **1** still possesses available pores filled with guest DMF and H_2O molecules (Fig. S3†). After removal of the guests, the solvent-accessible void volume is up to 23.6% as calculated by PLATON,[32] which is close to that observed in 8-fold interpenetrated $[Zn(oba)(pip)]_n$ (oba = 4,4′-oxybis(benzenedicarboxylate), pip = 4-pyridyl functionalized benzene-1,3-dicarbohydrazide) (27.2%)[33] but much larger than that in $[Zn(L^1)(1,4\text{-BDC})]\cdot H_2O$ (L^1 = *N*,*N*′-di(4-pyridyl) adipoamide; 1,4-H_2BDC = 1,4-benzenedicarboxylic acid) (4.9%).[34]

Stability test

To obtain porous MOFs materials, the solvent-exchange and vacuum heat treatment technique are usually used to removal of isolated solvent molecules. Therefore, the thermal stability of **1** was investigated firstly. As shown in the Fig. S4a,† the thermogravimetric analysis (TGA) of **1** shows an initial weight loss of 14.78% in the range of 120–260 °C, which may be attributed to the loss of one isolated DMF and three isolated H_2O molecules (calcd 14.83%). No further weight loss is observed below 305 °C, indicating a good thermal stability. Upon further heating, the framework begins to decompose and the final residue may be attributed to ZnO (obsd 9.45%, calcd 9.50%). The above results are also supported by the variable-temperature PXRD data (Fig. S4b†). Whereas the TGA of activated **1a** does not show any weight loss below 305 °C, indicating completely removing the isolated DMF and H_2O molecules and successfully obtaining a porous solvent-free MOF material.

Considering the practical application in aqueous media, the water stability of porous **1a** was further investigated in water, boiling water, as well as HCl and NaOH aqueous solution. As

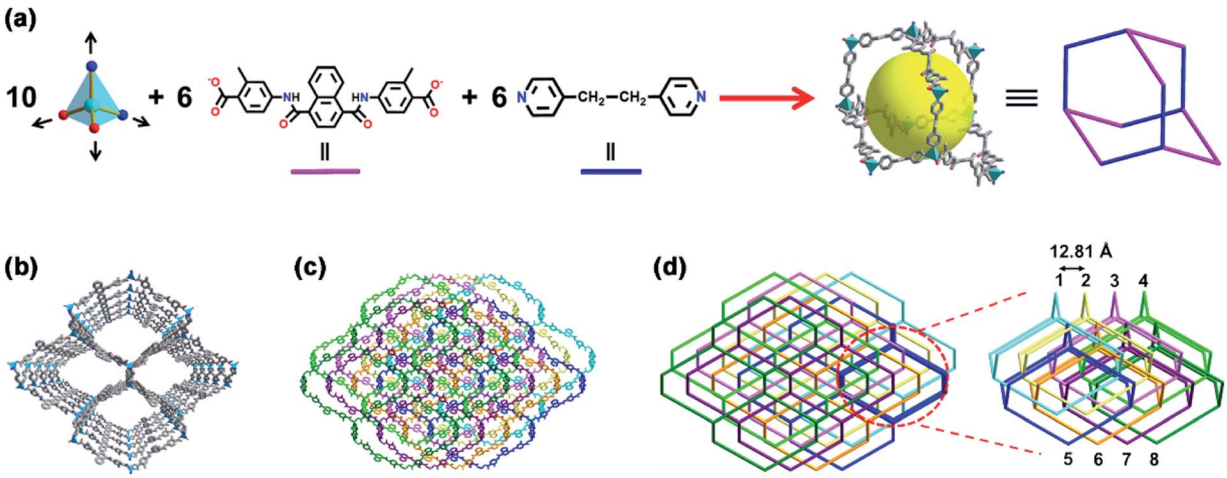

Fig. 2 Illustrating the structure of **1**: (a) the assembly of a single diamondoid cage. (b) A single non-interpenetrated 3D framework (c) 8-fold interpenetrated 3D framework. (d) The 8-fold interpenetrated topology with [4 + 4] mode.

shown in Fig. S5a,† PXRD patterns of **1a** after immersion in water at RT for two weeks and in boiling water for 72 h well match with those of untreated **1a**, demonstrating the high water stability. The further PXRD measurements of **1a** samples after treated by different HCl and NaOH aqueous solution exhibit that the diffraction peaks don't show apparently change with pH of 3–10 for 12 h, indicating the good water stability under these conditions; whereas the diffraction peaks start to disappear when pH < 2 or pH > 11, indicating the decomposition of **1a** occurs (Fig. 3a). Moreover, the water adsorption isotherms of **1a** in all five cycles almost overlap with that of origin one, further confirming the excellent water stability of **1a** (Fig. 3b). The introduction of methyl groups in H_2L ligand and high degree of interpenetrated structure may be the main factors in enhancing the water stability of **1a**, although it still exhibits a slight hydrophilic nature with water contact angle of 86° (Fig. S5b†).

Luminescence properties

MOFs constructed from d^{10} metal ions and electron-rich π-conjugated organic ligands are usually considered as the excellent luminescent materials. Thus, the luminescence property of **1a** dispersed in water was investigated at room temperature. As shown in Fig. S6,† MOF **1a** exhibits a strong emission peak appearing at 470 nm upon excitation at 340 nm. Compared with the free ligand H_2L, the emission peak of MOF **1a** displays a large red-shift about 66 nm, which may be assigned to the ligand-to-metal charge transfer (LMCT).[35–38]

Detection of metal ions

Considering the high water stability and good luminescent performance, MOF **1a** was applied to detect different metal ions in aqueous solution. In this work, a series of metal ions including Li^+, K^+, Na^+, Ni^{2+}, Co^{2+}, Zn^{2+}, Mg^{2+}, Cu^{2+} and Al^{3+}, were tested. As shown in Fig. 4a, the luminescence intensity of **1a** is obviously increased upon the addition of Al^{3+}, which is nearly 3 times of the initial luminescence intensity when the concentration of Al^{3+} is up to 167.0 μM. The other metal ions display ignored or slightly reduced the luminescence intensity of **1a** under the similar conditions.

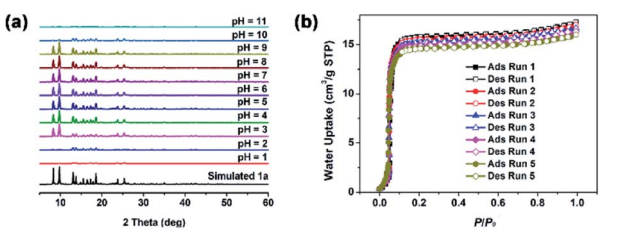

Fig. 3 (a) PXRD patterns of **1a** samples after treated by different HCl and NaOH aqueous solution with pH 1–11 for 12 h. (b) Water adsorption isotherm cycles of **1a** at 298 K.

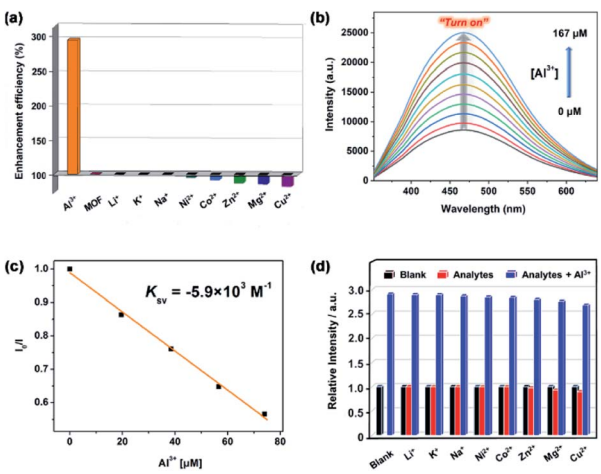

Fig. 4 (a) Enhancement efficiency of **1a** toward different metal ions. (b) Emission intensities of **1a** upon incremental addition of Al^{3+}. (c) SV plot of Al^{3+} at lower concentrations. (d) Selective detection of Al^{3+} in the presence of other interfering metal ions.

To further study sensing ability of **1a** toward Al^{3+}, the luminescence titrations experiments were performed. The pH is an important parameter in detection of Al^{3+}, because the speciation of Al^{3+} will be greatly affected by pH values. As shown in Fig. S7,† the Al^{3+} will be gradually hydrolysed to form $[Al(H_2O)_6]^{3+}$, $[Al(H_2O)_5(OH)]^{2+}$, $[Al(H_2O)_4(OH)_2]^{+}$, $Al(OH)_3$, $[Al(OH)_4]^{-}$ and so on, with the increase of pH value. Together with consideration of the water stability of **1a**, pH = 3 is the optimal detection for the present Al^{3+} detection. As shown in Fig. 4b, the luminescence intensity of **1a** at 470 nm progressively enhances with increasing the concentration of Al^{3+}. The enhanced luminescence efficiency of Al^{3+} is analysed by using the Stern–Volmer equation[18]: $I_0/I = K_{sv}[Q] + 1$, where $[Q]$ is the molar concentration of the analyte and K_{sv} is the enhancement constant (M^{-1}), I_0 and I are the luminescence intensities before and after addition of the analyte, respectively. As shown in Fig. 4c, the SV plot of Al^{3+} is nearly linear at low concentration and the enhancement constant is about $5.9 \times 10^3\ M^{-1}$, which is very close to the reported value of Zn-MOF for detection of Al^{3+} ($6.04 \times 10^3\ M^{-1}$).[39] Based on the slope of the calibration curve (K) and the standard deviation (δ) for three repeated luminescence measurements of blank solutions, the limit of detection (LOD, $3\delta/K$) of **1a** toward Al^{3+} is calculated to be 41.9 ppb, which is better than the reported luminescent MOF sensors for Al^{3+} detection (Table S3†). It is worth noting that the present LOD toward Al^{3+} (41.9 ppb) is much lower than the recommended level of Al^{3+} in drinking water from the United States Environmental Protection Agency (200 ppb). The selective detection of Al^{3+} in the presence of other interfering metal ions was also examined. As shown in Fig. 4d, the emission intensity of **1a** almost does not change in the presence of other interfering metal ions but is significantly enhanced upon the introduction of Al^{3+} into the mixture of **1a** and other interfering metal ions, which indicates that the interference from other metal ions could be neglected and confirms the highly selective detecting ability of **1a** toward Al^{3+}. In addition, MOF **1a** could be regenerated and reused by centrifuging the dispersed solution after sensing of Al^{3+} and washing with water several times, which could almost regain the initial luminescence intensity over five cycles (Fig. S8†). Thus, MOF **1a** could be used as a highly selective and reversible "turn-on" luminescent sensor for the detection of Al^{3+} in practical applications.

To better understand the luminescence enhancement effect of **1a** toward Al^{3+}, an explanation of the possible mechanism was attempted. As known, the luminescent sensing effect of MOFs caused by metal ions usually derives from the damage of the MOF structures,[40] the cation changes between metal centres of MOFs and the target cations,[41] or the host–guest interactions between MOFs and analytes.[42,43] As shown in Fig. 5a, the PXRD patterns with addition of Al^{3+} are similar to that of experimental **1a**, suggesting that the framework maintains its integrity. Thus, the turn-on sensing mechanism of **1a** toward Al^{3+} could not be due to the collapse of the MOF structure. Furthermore, the luminescence enhanced mechanism of **1a** toward Al^{3+} should also not result from cation-exchange due to the neutral framework of **1a**. The XPS data exhibit that there exist Al^{3+} after the luminescence titration experiments of **1a** (Fig. S9†). Therefore,

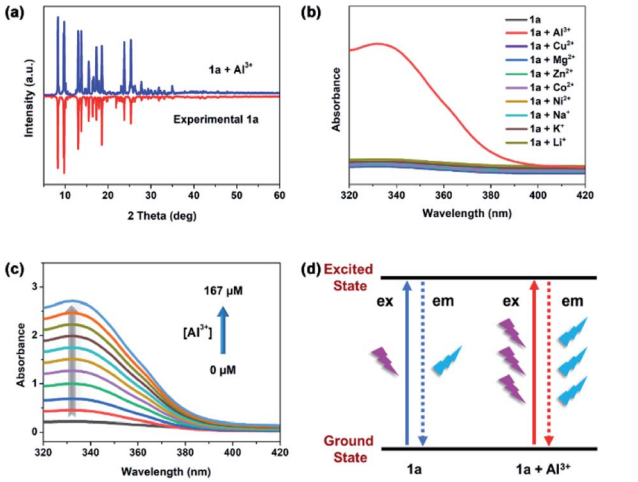

Fig. 5 (a) PXRD patterns of **1a** and **1a** + Al^{3+}. (b) UV-vis absorption spectra of **1a** upon addition of various metal ions. (c) UV-vis absorption spectra of **1a** upon incremental addition of Al^{3+}. (d) The schematic illustration of ACE effect for **1a** + Al^{3+}.

the sensing mechanism may be attributed to the host–guest interactions between Al^{3+} and the framework of **1a**. In IR spectra, the characteristic C=O vibration band of acylamide group is shifted from 1664 (for **1a**) to 1630 cm^{-1} (for **1a** + Al^{3+}) and a new absorption peak is observed at 590 cm^{-1} in **1a** + Al^{3+}, both indicate the presence of Al → O contact between Al^{3+} and the acylamide C=O units (Fig. S10†). As shown in Fig. 5b, the UV-vis spectra show that the absorbance of **1a** in range of 320–400 nm almost doesn't change with addition of different metal cations except Al^{3+}, which indicates that the sensing mechanism may be the absorbance caused enhancement (ACE) effect.[44] To eliminate the influence of Al^{3+} itself, the Al^{3+} absorption spectrum was also measured in aqueous solution (Fig. S11†). The result shows that the Al^{3+} have no absorbance in the range of 320–400 nm, so we rationally believe that the significant absorbance enhancement of **1a** should derive from the complexation of **1a** and Al^{3+}. In addition, the UV-vis titration experiments of **1a** toward Al^{3+} were performed to further elucidate the ACE mechanism. As show in Fig. 5c, the absorbance of **1a** gradually enhances with the increasing of Al^{3+} concentrations, which is well consistent with the above luminescence titration results. However, both absorption and emission wavelengths of **1a** basically do not change in UV-vis (Fig. 5c) and luminescence (Fig. 4b) titration experiments. Therefore, we speculated the luminescence enhancement mechanism of **1a** toward Al^{3+} should be that **1a** + Al^{3+} absorbs more energy than pristine **1a** from the light source in the excitation process, and then it will release more energy than **1a** in the emission process, thus yielding the luminescent "turn-on" effect (Fig. 5d). The similar phenomena were also observed in other luminescent MOF sensors for detection of Al^{3+}.[43,44]

Detection of antibiotics

The similar procedure was used to investigate the sensing ability of **1a** for detecting different antibiotics including

sulfanitran (SNT), sulfadiazine (SDZ), sulfamethazine (SMZ), sulfamethoxazole (SMX), roxithromycin (ROX), azithromycin (AZM) and gentamicin (GEN) in aqueous media. As shown in Fig. 6a, MOF **1a** presents a high quenching efficiency about 96.8% toward SNT, while the quenching efficiencies toward other antibiotics are very low.

To further study sensing ability of **1a** toward SNT, the luminescence titrations experiments were performed. As shown in Fig. 6b, the luminescence intensity of **1a** progressively decreases with the gradual addition of SNT. The S–V equation can also be employed to analysed the quenching efficiency of SNT according to the literature.[18] As shown in Fig. 6c, the SV plot for SNT was nearly linear below 74.1 μM but subsequently deviated from linearity and bent upward at higher concentrations. The nonlinear nature of SV plot of SNT may be ascribed to an energy-transfer process or self-absorption.[45–48] The quenching constant is calculated to be 2.8×10^4 M^{-1} for SNT, which is close to the reported value of luminescent MOF sensors toward antibiotics analytes.[49–52] The LOD could reach 20.2 ppb based on $3\delta/K$, showing the highly sensitive sensing ability to SNT for **1a**. The selective detection of SNT in the presence of other interfering antibiotics was also examined. As shown in Fig. 6d, the emission intensity of **1a** almost does not change in the presence of other interfering antibiotics but is significantly quenched upon the introduction of SNT into the mixture of **1a** and other interfering antibiotics, which indicates that the interference from other antibiotics could be neglected and confirms the highly selective detecting ability of **1a** toward SNT. In addition, MOF **1a** could be also regenerated and reused by centrifuging the dispersed solution after sensing of SNT and washing with water several times, which could almost regain the initial luminescence intensity over five cycles (Fig. S12†). Thus, the MOF **1a** could be used as a highly selective and reversible "turn-off" luminescent sensor for the detection of SNT in practical applications.

In order to better understand the luminescence quenching effect of **1a** toward SNT, the quenching mechanism was investigated. Taking account of the strong π-conjugated effect of H_2L ligand and the nature of electron deficiency of analytes, the photoinduced electron transfer (PET) mechanism is proposed. Generally, the excited electrons lying in the higher LUMO of the luminescent ligand are transferred to the lower LUMO of the electron-deficient analytes, resulting in luminescence quenching. The lower the LUMO energy of analytes, the more easily the electrons are transferred to the acceptor.[49] As revealed by Fig. 7a and Table S4,† the calculated LUMO energies are in good agreement with the maximum quenching efficiency observed in SNT, but the order of the experimental quenching efficiencies is not fully in accordance with the LUMO energies of the other antibiotics. Therefore, the PET might be not the only mechanism for luminescence quenching in the current system. To further ascertain the possible luminescence quenching reason, the excitation spectrum of **1a** and the UV-vis absorption spectra of various antibiotics were investigated. As shown in Fig. 7b, the absorption spectrum of SNT has the greatest degree of overlapping with the excitation spectrum of **1a**, but no effective spectral overlaps are observed between **1a** and other antibiotics. Thus, the excitation energy from the light source could be partially absorbed by SNT, which causes the luminescence weakening or quenching. The above facts suggest that the inner filter effect (IFE) may be another reason for the luminescence quenching of SNT in this system. Obviously, the coexistence of PET and IFE between **1a** and SNT leads to the "turn-off" luminescent effect, and yields highly sensitive and selective detection of SNT in aqueous solution.

Application to real water samples

The excellent water stability and good luminescent sensing feature inspired us to explore **1a** as an effective chemical sensor for determining the concentrations of Al^{3+} and SNT in real water samples, such as tap water, the Dongchang Lake and the Yellow River. The water samples spiked with different concentrations of Al^{3+} and SNT were analysed with the proposed method in this work. As shown in Table S5,† the recoveries are 93.7 to 107.6% with relative standard deviation (RSD) variations from 1.1 to 4.8%, which display satisfactory recoveries and acceptable accuracies. The above results exhibit the feasibility and reliability of the proposed luminescent analysis method for the accurate determination of Al^{3+} and SNT in environmental water matrices.

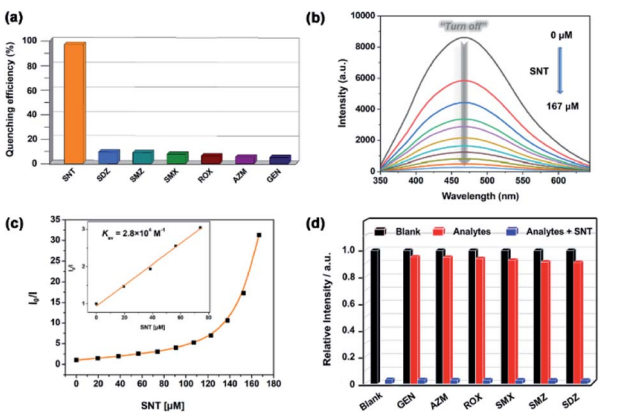

Fig. 6 (a) Quenching efficiency of **1a** toward different antibiotics. (b) Emission intensities of **1a** upon incremental addition of SNT. (c) SV plot of SNT. Inset: SV plot at lower concentrations. (d) Selective detection of SNT in the presence of other interfering antibiotics.

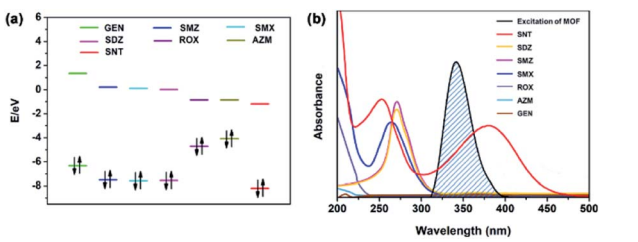

Fig. 7 (a) HOMO and LUMO energies of antibiotics arranged in the descending order of LUMO energy. (b) Spectral overlap of the excitation spectrum of **1a** with the absorption spectra of different antibiotics.

Conclusions

In summary, a new luminescent Zn-MOF was successfully synthesized based on an elaborately designed methyl-decorated acylamide-containing dicarboxylate ligand H_2L. The as-synthesized MOF **1** shows a three-dimensional 8-fold [4 + 4] interpenetrated diamondoid framework with isolated DMF and water molecules in the pores, in which the uncoordinated acylamide groups are found and facilitated the Zn-MOF to recognize analyte molecules. The activated MOF **1a** featured an enhanced water stability due to the introduction of hydrophobic methyl groups in H_2L ligand and possession of the high degree of interpenetration structure. The luminescence sensing experiments showed that **1a** could behave as a bi-responsive chemical sensor for "turn-on" and "turn-off" luminescent detection of Al^{3+} and SNT in aqueous media, respectively. The sensing mechanisms have also been discussed. Furthermore, the practical application feasibility of the present luminescent analysis method for the sensing of Al^{3+} and SNT in real water samples was demonstrated. To our knowledge, this represents the first example of bi-responsive MOF sensor for "turn-on" and "turn-off" luminescent detection of Al^{3+} and SNT in aqueous media. The present study will provide a new insight in design and syntheses of excellent water-stable luminescent MOFs as bi-responsive luminescent sensors for monitoring metal ions and antibiotics pollutants in the environmental water matrices.

Author contributions

X. T. Gao and X. H. Wang contributed equally to this paper.

Conflicts of interest

There are no conflicts to declare.

Acknowledgements

This work was supported by the National Natural Science Foundation of China (Grant No. 21771096).

References

1 W. Adams, R. Blust, R. Dwyer, D. Mount, E. Nordheim, P. H. Rodriguez and D. Spry, *Environ. Toxicol. Chem.*, 2020, **39**, 48–59.
2 M. Qiao, G. G. Ying, A. C. Singer and Y. G. Zhu, *Environ. Int.*, 2018, **110**, 160–172.
3 Z. Li, M. Li, Z. Zhang, P. Li, Y. Zang and X. Liu, *Ecotoxicol. Environ. Saf.*, 2020, **199**, 110668.
4 K. M. Sta Ana, J. Madriaga and M. P. Espino, *Environ. Pollut.*, 2021, **275**, 116624.
5 E. Žerovnik, *Curr. Alzheimer Res.*, 2010, **7**, 74–83.
6 S. C. Bondy, *Neurotoxicology*, 2010, **31**, 575–581.
7 K. M. A. Akhali, A. K. Alzomar, N. A. Khan and S. S. Alavudeen, *Pharm. Globale*, 2013, **1**, 1–4.
8 Y. Wang, *Advances in Social Science, Education and Humanities Research*, 2018, vol. 283, pp. 958–960.
9 M. Bacanlı and N. Başaran, *Food Chem. Toxicol.*, 2019, **125**, 462–466.
10 S. Murko, J. Ščančar and R. Milačič, *J. Anal. At. Spectrom.*, 2011, **26**, 86–93.
11 M. D. Amos and P. E. Thomas, *Anal. Chim. Acta*, 1965, **32**, 139–147.
12 D. A. Bohm, C. S. Stachel and P. Gowik, *Anal. Chim. Acta*, 2010, **672**, 103–106.
13 M. D. Allendorf, C. A. Bauer, R. K. Bhakta and R. J. T. Houk, *Chem. Soc. Rev.*, 2009, **38**, 1330–1352.
14 T. Rasheed and F. Nabeel, *Coord. Chem. Rev.*, 2019, **401**, 213065.
15 Y. Liu, X. Y. Xie, C. Cheng, Z. S. Shao and H. S. Wang, *J. Mater. Chem. C*, 2019, **7**, 10743–10763.
16 Y. Yu, Y. Wang, H. Yan, J. Lu, H. Liu, Y. Li, S. Wang, D. Li, J. Dou, L. Yang and Z. Zhou, *Inorg. Chem.*, 2020, **59**, 3828–3837.
17 S. Pramanik, C. Zheng, X. Zhang, T. J. Emge and J. Li, *J. Am. Chem. Soc.*, 2011, **133**, 4153–4155.
18 X. Zhang, X. Luo, N. Zhang, J. Wu and Y.-Q. Huang, *Inorg. Chem. Front.*, 2017, **4**, 1888–1894.
19 N. C. Burtch, H. Jasuja and K. S. Walton, *Chem. Rev.*, 2014, **114**, 10575–10612.
20 C. Wang, X. Liu, N. Keser Demir, J. P. Chen and K. Li, *Chem. Soc. Rev.*, 2016, **45**, 5107–5134.
21 M. Ding, X. Cai and H. L. Jiang, *Chem. Sci.*, 2019, **10**, 10209–10230.
22 G. Férey, C. Mellot-Draznieks, C. Serre, F. Millange, J. Dutour, S. Surblé and I. Margiolaki, *Science*, 2005, **309**, 2040–2042.
23 H. Jiang, K. Yang, X. Zhao, W. Zhang, Y. Liu, J. Jiang and Y. Cui, *J. Am. Chem. Soc.*, 2021, **143**, 390–398.
24 K. Wang, H. Huang, X. Zhou, Q. Wang, G. Li, H. Shen, Y. She and C. Zhong, *Inorg. Chem.*, 2019, **58**, 5725–5732.
25 H. Jasuja and K. S. Walton, *Dalton Trans.*, 2013, **42**, 15421–15426.
26 H. Jasuja, Y. Jiao, N. C. Burtch, Y. G. Huang and K. S. Walton, *Langmuir*, 2014, **30**, 14300–14307.
27 G. M. Sheldrick, *Acta Crystallogr C Struct. Chem.*, 2015, **71**, 3–8.
28 L. Carlucci, G. Ciani, D. M. Proserpio and S. Rizzato, *Chem.–Eur. J.*, 2002, **8**, 1520–1526.
29 H. Kim and M. P. Suh, *Inorg. Chem.*, 2005, **44**, 810–812.
30 X.-M. Guo, Y.-N. Yan, H.-d. Guo and N. Wang, *Inorg. Chem. Commun.*, 2015, **61**, 105–108.
31 J. Li, Y. Ren, C. Qi and H. Jiang, *Dalton Trans.*, 2017, **46**, 7821–7832.
32 A. L. Spek, *Acta Crystallogr D Biol. Crystallogr.*, 2009, **65**, 148–155.
33 K. Roztocki, F. Formalik, A. Krawczuk, I. Senkovska, B. Kuchta, S. Kaskel and D. Matoga, *Angew. Chem., Int. Ed.*, 2020, **59**, 4491–4497.
34 J.-J. Cheng, Y.-T. Chang, C.-J. Wu, Y.-F. Hsu, C.-H. Lin, D. M. Proserpio and J.-D. Chen, *CrystEngComm*, 2012, **14**, 537–543.
35 W. P. Lustig, S. Mukherjee, N. D. Rudd, A. V. Desai, J. Li and S. K. Ghosh, *Chem. Soc. Rev.*, 2017, **46**, 3242–3285.

36 Y. Guo, X. Feng, T. Han, S. Wang, Z. Lin, Y. Dong and B. Wang, *J. Am. Chem. Soc.*, 2014, **136**, 15485–15488.
37 S. Dawood, A. Dorris, K. Davis, N. I. Hammer and H. Rathnayake, *J. Phys. Chem. C*, 2021, **125**, 792–802.
38 P. Majee, D. K. Singha, S. K. Mondal and P. Mahata, *Photochem. Photobiol. Sci.*, 2019, **18**, 1110–1121.
39 M. Arici, *New J. Chem.*, 2019, **43**, 3690–3697.
40 L.-H. Cao, F. Shi, W.-M. Zhang, S.-Q. Zang and T. C. Mak, *Chem.–Eur. J.*, 2015, **21**, 15705–157112.
41 C.-X. Yang, H.-B. Ren and X.-P. Yan, *Anal. Chem.*, 2013, **85**, 7441–7446.
42 S.-Y. Zhu and B. Yan, *Dalton Trans.*, 2018, **47**, 1674–1681.
43 X.-M. Tian, S.-L. Yao, C.-Q. Qiu, T.-F. Zheng, Y.-Q. Chen, H. Huang, J.-L. Chen, S.-J. Liu and H.-R. Wen, *Inorg. Chem.*, 2020, **59**, 2803–2810.
44 M. Wang, L. Guo and D. Cao, *Sens. Actuators, B*, 2018, **256**, 839–845.
45 Q. F. Zhang, A. J. Geng, H. N. Zhang, F. L. Hu, Z. H. Lu, D. Z. Sun, X. L. Wei and C. L. Ma, *Chem.–Eur. J.*, 2014, **20**, 4885–4890.
46 Z.-Q. Shi, Z.-J. Guo and H.-G. Zheng, *Chem. Commun.*, 2015, **51**, 8300–8303.
47 W. Yan, C. Zhang, S. Chen, L. Han and H. Zheng, *ACS Appl. Mater. Interfaces*, 2017, **9**, 1629–1634.
48 Y. Du, H. Yang, R. Liu, C. Shao and L. Yang, *Dalton Trans.*, 2020, **49**, 13003–13016.
49 B. Wang, X.-L. Lv, D. Feng, L.-H. Xie, J. Zhang, M. Li, Y. Xie, J.-R. Li and H.-C. Zhou, *J. Am. Chem. Soc.*, 2016, **138**, 6204–6216.
50 X.-D. Zhu, K. Zhang, Y. Wang, W.-W. Long, R.-J. Sa, T.-F. Liu and J. Lü, *Inorg. Chem.*, 2018, **57**, 1060–1065.
51 C. Li, C. Zeng, Z. Chen, Y. Jiang, H. Yao, Y. Yang and W. T. Wong, *J. Hazard. Mater.*, 2020, **384**, 121498.
52 C. Li, W. Yang, X. Zhang, Y. Han, W. Tang, T. Yue and Z. Li, *J. Mater. Chem. C*, 2020, **8**, 2054–2064.